Shear-induced buckling of a thin elastic disk undergoing spin-up

John E. Sader[1,2], Mélanie Delapierre[3], and Sergio Pellegrino[3]

[1]*ARC Centre of Excellence in Exciton Science, School of Mathematics and Statistics, The University of Melbourne, Victoria 3010, Australia*

[2]*Department of Physics, California Institute of Technology, Pasadena, CA 91125, USA*

[3]*Graduate Aerospace Laboratories, California Institute of Technology, Pasadena, CA 91125, USA*

(Dated: January 7, 2019)

Abstract

The stability of a spinning thin elastic disk has been widely studied due to its central importance in engineering. While the plastic deformation and failure of an annular disk mounted on a rigid and accelerating circular shaft are well understood, shear-induced elastic buckling of the disk due to this 'spin-up' is yet to be reported. Here, we calculate this buckling behavior within the framework of the Föppl–von Kármán equations and give numerical results as a function of the disk's aspect ratio (inner-to-outer radius) and Poisson's ratio. This shows that shear-induced elastic buckling can dominate plastic failure in many cases of practical interest. When combined with existing theory for plastic failure, the results of the present study provide foundation results for a multitude of applications including the characterization of accelerating compact disks and deployment of space sails by centrifugal forces.

I. INTRODUCTION

Rotating thin elastic disks are widely used in engineering, which has motivated numerous investigations into their mechanical stability and dynamics [1]. These include studies of disk-brake squeal [2], vibration and friction-induced instabilities [3], stability under transverse loading [4, 5], buckling under a gravitational load [6, 7], finite strain analysis of anisotropic rotating disks [8], plastic yielding of rotating disks [9–11], elastoplasic buckling of stationary anisotropic disks [12], parametric resonance [13] and the effect of rigid body tilt [14]. It is now well understood that these rotating structures induce internal stresses that can lead to plastic deformation and/or fracture. This is perhaps most strikingly evident in the mechanical failure of a thin circular disk that is rotating at high angular velocity, e.g., a rotating compact disk [15].

Directly related to these problems, which involve steady rotation, is the angular acceleration or 'spin-up' of a thin elastic disk. Early work by Stern [16] and Tang [17] determined the shear stress in a thin annular disk that is clamped at its inner edge to an accelerating rigid circular shaft, with its outer edge free; this solution built on established results for the normal stresses [1]. Tang [17] showed that angular acceleration of the rigid circular shaft about its axis leads to maximal shear stress at the disk's inner edge. Subsequent work by Reid [18] utilized this derived stress state to study the stability of a rotationally accelerating disk due to plastic deformation [18], extending previous results for the steady rotation problem discussed above.

A problem related to the stability of a rotationally accelerating elastic disk is stability of a thin annular disk subjected to a time-independent (static) shear. This problem was first calculated by Dean [19] who considered the inner and outer edge of the disk to be rigidly clamped and subject to different static angular displacements. The resulting shear stress and elastic buckling behavior of the disk displayed good agreement with measurements. This initial work was extended more recently to include polar-orthotropic plates [20] and various disk boundary conditions [21]. In the latter study, a specified and fixed shear stress of $\tau/(2\pi r^2)$, where τ is the torsional moment and r is the radial coordinate from the disk center, is applied; see Eq. (7) of Ref. [21]. A range of canonical boundary conditions for the inner and outer edges of the disk are reported, e.g., clamped-clamped, clamped-simply supported, clamped-free etc. But the assumed shear stress in that study is for uniform loading at the

inner and outer edges of the disk, which is apparently contradictory to the usual definitions of some of these boundary conditions. For example, the zero traction condition at a free edge strictly requires the shear stress to vanish at that position. Thus, the various boundary conditions studied in Ref. [21] must be considered in that context. Work has also focused on the practical case of tension (in the radial direction) between the inner and outer edges of the disk [22–25]. These studies show that raising this applied tension increasingly confines the buckled mode to the inner edge of the disk.

The spin-up (angular acceleration) of a thin annular disk, such as a compact disk, generates a shear stress which in principle should lead to buckling behavior similar to that observed for static shear of an annular disk [19–25]. Importantly, the buckling behavior of a disk undergoing spin-up cannot be determined from these previously reported static shear solutions [19–25]—due to the fundamental difference in boundary conditions, which does not allow for a mapping of the present problem onto these published solutions; this is discussed in Section III D. Furthermore, while calculation of the plastic failure of an elastic disk undergoing spin-up has been performed (see above), the corresponding shear-induced buckling of a thin elastic disk in spin-up is yet to be reported. This therefore represents a significant omission in the applied mechanics literature of a canonical problem that is relevant across a multitude of engineering applications; the relative importance of shear-induced elastic buckling and plastic failure is examined in Section III C.

The aim of this article is to fill this gap in the literature and provide numerical results that can be used in application. This calculation is achieved within the framework of the Föppl–von Kármán equations [26], which intrinsically allows a general plane stress distribution to be specified; see Ref. [27] for a discussion and critique of these equations. As in studies that investigated static shear-induced buckling of an annular disk [19–25], the effects of body forces normal to the disk surface (e.g., gravity) are ignored. This is relevant to applications in microgravity environments and also when the induced in-plane stress due to rotation greatly exceeds internal stresses generated by any external body force. We show that the plane stress distribution in the accelerating disk [1, 16, 17] is decoupled from the subsequent buckling problem; this differs from a rotating circular disk that is loaded by forces normal to its surface [7]. Results are given for the critical angular acceleration at which buckling occurs for both zero and nonzero instantaneous angular velocity of the disk. This is performed as a function of the disk's aspect ratio (inner-to-outer radius) and Poisson's ratio; see Fig. 1.

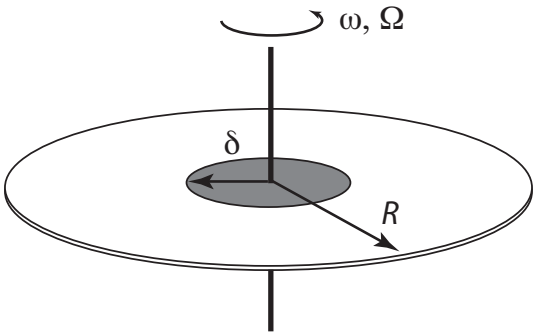

FIG. 1. Schematic illustration of the thin elastic disk showing its inner and outer radii. It is rigidly clamped at its inner radius, which is moving with angular velocity, ω, and acceleration, Ω, about the central axis of the disk. The disk is composed of an isotropic elastic material and its geometric aspect ratio is $a \equiv \delta/R$.

These results for shear-induced elastic buckling are then compared to existing literature for plastic failure, which shows that both mechanisms must be considered in the design of rotating disks. The stability of very thin disks such as floppy disk is found to be dictated by shear-induced elastic buckling. The post-buckling behavior of the annular disk is not considered, i.e., we focus on the buckling loads and their associated mode shapes.

II. ANALYSIS

A schematic illustration of the thin elastic disk and its rotary motion is given in Fig. 1. The buckling behavior of this disk is to be solved using the Föppl–von Kármán equations [26, 27] for a thin elastic plate:

$$D\nabla^4 w = h\nabla \cdot (\mathbf{T} \cdot \nabla w)\,, \tag{1}$$

$$\nabla \cdot \mathbf{T} = -\rho \mathbf{b}, \tag{2}$$

where $D \equiv Eh^3/(12[1-\nu^2])$ is the flexural rigidity of the plate (disk), E, ν, ρ and h are its Young's modulus, Poisson's ratio, density and thickness, respectively, w is the displacement function normal to the disk, $\mathbf{T}$ is the in-plane stress tensor in the disk and $\mathbf{b}$ is the applied body force per unit mass. We consider the problem in the rotating (non-inertial) frame of the disk which then experiences an instantaneous body force per unit mass,

$$\mathbf{b} = r\left(\omega^2 \hat{\boldsymbol{r}} - \Omega\hat{\boldsymbol{\phi}}\right), \tag{3}$$

where Ω and ω are the instantaneous angular acceleration and angular velocity of the disk, respectively, r and ϕ are the radial and azimuthal coordinates in the disk's plane, respectively, and $\hat{\boldsymbol{r}}$ and $\hat{\boldsymbol{\phi}}$ are the corresponding basis vectors.

While the in-plane stress evolves in time as the disk spins up, this stress is always in a state of quasi-equilibrium within the framework of the present thin plate theory; a result that we prove in Section II A. Solving the corresponding equilibrium equation, Eq. (2), then gives the results reported in Refs. [1, 16, 17]; this solution is reproduced in Appendix A for convenience. The quasi-equilibrium assumption is justified provided the time scale for stress to propagate through the disk is relatively small, i.e., $\Omega \ll E/(\rho R^2)$, where ρ and R are the disk density and radius, respectively. This condition arises from a scaling analysis of Navier's equation and is always satisfied for a disk of infinitesimal thickness—a primary assumption underlying Eq. (1)—at its buckling point; see Section II A for a discussion of the practical relevance of this condition. Hence, the quasi-equilibrium property of the in-plane stress distribution is formally consistent with Eq. (1).

The problem is non-dimensionalized using the following scales,

$$r \sim R, \qquad T_{rr},\, T_{\theta\theta} \sim \rho\,\omega^2 R^2, \qquad T_{r\phi} \sim \rho\,\Omega R^2, \tag{4}$$

from which Eq. (1) becomes

$$\nabla^4 w = \bar{\Omega}\left(\frac{\partial w}{\partial \phi} + 2T_{r\phi}\triangle w_{r\phi}\right) - \bar{\omega}^2\left(r\frac{\partial w}{\partial r} - T_{rr}\triangle w_{rr} - T_{\phi\phi}\triangle w_{\phi\phi}\right), \tag{5}$$

where

$$\triangle w_{rr} \equiv \frac{\partial^2 w}{\partial r^2}, \qquad \triangle w_{\phi\phi} \equiv \frac{1}{r}\frac{\partial w}{\partial r} + \frac{1}{r^2}\frac{\partial^2 w}{\partial \phi^2}, \qquad \triangle w_{r\phi} \equiv \frac{1}{r}\frac{\partial^2 w}{\partial r \partial \phi} - \frac{1}{r^2}\frac{\partial w}{\partial \phi}, \tag{6}$$

with all variables referring to their dimensionless quantities, where the dimensionless angular acceleration and angular velocity are respectively given by

$$\bar{\Omega} \equiv \frac{\rho h R^4 \Omega}{D}, \qquad \bar{\omega}^2 \equiv \frac{\rho h R^4 \omega^2}{D}. \tag{7}$$

Equation (5) is to be solved for w, subject to the clamped boundary condition at the disk's inner edge,

$$w|_{r=a} = \left.\frac{\partial w}{\partial r}\right|_{r=a} = 0, \tag{8}$$

and the corresponding free-edge condition at the outer edge:

$$\left[\frac{\partial^2 w}{\partial r^2} + \nu\left(\frac{1}{r}\frac{\partial w}{\partial r} + \frac{1}{r^2}\frac{\partial^2 w}{\partial \phi^2}\right)\right]_{r=1} = \left[\frac{\partial}{\partial r}\nabla^2 w + \frac{1-\nu}{r}\frac{\partial^2}{\partial r \partial \phi}\left(\frac{1}{r}\frac{\partial w}{\partial \phi}\right)\right]_{r=1} = 0. \tag{9}$$

Due to linearity, Eq. (5) is solved using the ansatz

$$w(r,\phi) = W(r)\exp\left(\mathrm{i}n\phi\right), \tag{10}$$

where n is an integer (periodicity in ϕ) and i is the usual imaginary unit; the required (real-valued) buckled mode is specified by the real (or imaginary) part of Eq. (10). Substituting Eq. (10) into Eqs. (5), (8) and (9) produces the required eigenvalue problem in the form of a fourth-order ordinary differential equation for $W(r)$,

$$\begin{aligned}\frac{1}{r^2}\frac{d}{dr}\left(r^2\frac{d^3W}{dr^3}\right) - \frac{2n^2+1}{r}\frac{d}{dr}\left(\frac{1}{r}\frac{dW}{dr}\right) + \frac{n^2(n^2-4)}{r^4}W \\ = \bar{\omega}^2\left(T_{rr}\frac{d^2W}{dr^2} - \left[r - \frac{T_{\phi\phi}}{r}\right]\frac{dW}{dr} - \frac{n^2T_{\phi\phi}}{r^2}W\right) + in\bar{\Omega}\left(\frac{2T_{r\phi}}{r}\frac{dW}{dr} + \left[1 - \frac{2T_{r\phi}}{r^2}\right]W\right),\end{aligned} \tag{11}$$

with associated boundary conditions,

$$W(a) = \left.\frac{dW}{dr}\right|_{r=a} = 0, \tag{12}$$

$$\left[\frac{d^2W}{dr^2} + \nu\left(\frac{dW}{dr} - n^2W\right)\right]_{r=1} = 0, \tag{13}$$

$$\left[\frac{d^3W}{dr^3} + \frac{d^2W}{dr^2} + \left(n^2\left[\nu-2\right]-1\right)\frac{dW}{dr} + n^2\left(3-\nu\right)W\right]_{r=1} = 0, \tag{14}$$

where Eq. (12) is the clamp boundary condition at $r = a$, while Eqs. (13) and (14) coincide with the free edge condition at $r = 1$.

This eigenvalue problem is to be solved for fixed angular velocity, $\bar{\omega}$, yielding the critical acceleration, $\bar{\Omega}$, for buckling. Since this problem depends on the mode number, n, the required buckled mode (and angular acceleration) is specified by that which produces the smallest $\bar{\Omega}$.

A. Condition for quasi-static in-plane stress

The above-stated condition, $\Omega \ll E/(\rho R^2)$, for a quasi-equilibrium in-plane stress state is identical to

$$\bar{\Omega} \ll 12\left(1-\nu^2\right)\left(\frac{R}{h}\right)^2, \tag{15}$$

under the scalings defined in Eq. (7). Since the dimensionless buckling acceleration $\bar{\Omega} \equiv \bar{\Omega}_{\text{buckle}}$ is finite (see Section III), this inequality always holds in the limit $h/R \to 0$; this limit is implicit in Eq. (1). Importantly, it holds for many applications, e.g., a floppy

disk exhibits a typical radius-to-thickness ratio of $R/h = 1{,}000$, leading to the requirement, $\bar{\Omega} \ll 10^7$; which is well-satisfied in the results to be presented in Section III.

III. RESULTS AND DISCUSSION

Equations (11) – (14) are solved numerically using a spectral method involving Chebyshev polynomials [28]; the number of polynomials is systematically increased to achieve convergence better than 99.99%. This numerical method represents the radial displacement function, $W(r)$, as an expansion in Chebyshev polynomials with (to be determined) unknown coefficients. Substituting this expansion into Eqs. (11) – (14), and using the orthogonal properties of Chebyshev polynomials, enables the eigenvalue problem to be converted into an equivalent matrix system involving the unknown coefficients. Standard linear solvers are then used to determine the eigenvalue and associated coefficients in the Chebyshev polynomial expansion—giving the required buckling accelerations and associated modes (via Eq. (10)). We employ the Mathematica implementation in Ref. [28] of this spectral method. For each disk aspect ratio, a (defined in Fig. 1), and Poisson's ratio, ν, the buckling acceleration, $\bar{\Omega}$, is calculated for a range of mode numbers, $n \geq 1$, as a function of angular velocity, $\bar{\omega}$. The required (lowest) buckling acceleration, $\bar{\Omega} \equiv \bar{\Omega}_{\text{buckle}}$, and associated mode number, $n \equiv n_{\text{buckle}}$, at a specified angular velocity, $\bar{\omega}$, are then evaluated using a simple numerical search procedure—this involves computing the buckling accelerations for a range of mode numbers, n, and identifying the mode with the lowest acceleration. Results of this calculation are given in Fig. 2.

A. Buckling acceleration

Figures 2(A, B) give results for $\bar{\Omega}_{\text{buckle}}$ with a Poisson's ratio of $\nu = 1/4$, whereas Figs. 2(C, D) illustrate the dependence on Poisson's ratio over the range $0 \leq \nu \leq 1/2$, which is found to be weak. This insensitivity of $\bar{\Omega}_{\text{buckle}}$ to Poisson's ratio, ν, (and similarly for the flexural rigidity, D) is advantageous in practice because it allows for robust design and application without the need for precise knowledge of ν.

The results in Figs. 2(A, C) show that increasing the disk aspect ratio, a, enhances the buckling acceleration, $\bar{\Omega}_{\text{buckle}}$. This is expected because an increase in aspect ratio, a—

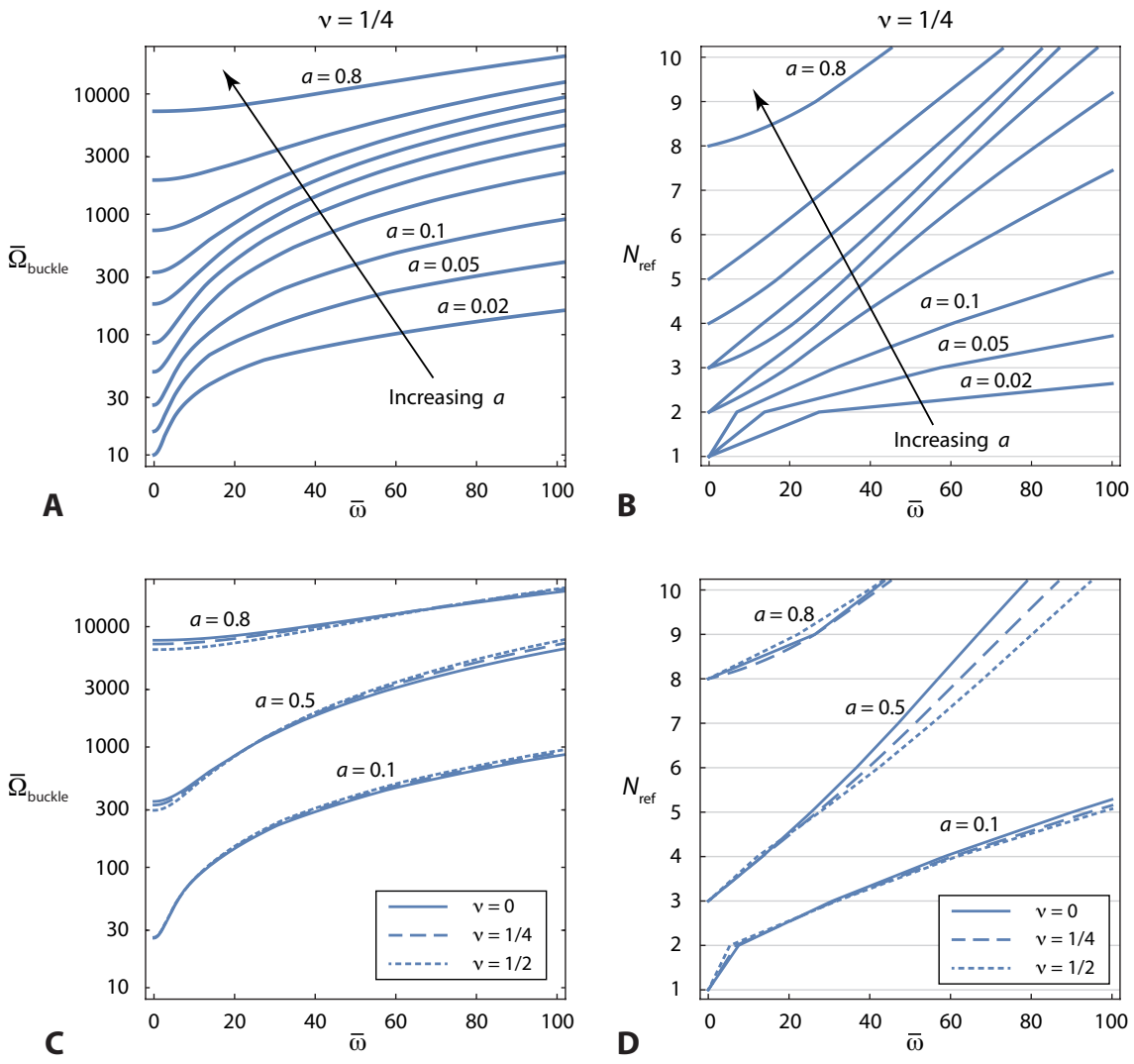

FIG. 2. Numerical results for the buckling acceleration, $\bar{\Omega}_{\text{buckle}}$, and associated mode number, $n_{\text{buckle}} = \lfloor N_{\text{ref}} \rfloor$, (where $\lfloor ... \rfloor$ specifies the integer part), for a thin annular disk rotating with instantaneous angular velocity, $\bar{\omega}$. Results for Poisson's ratio of $\nu = 1/4$ and aspect ratios, $a = 0.02, 0.05, 0.1, 0.2, 0.3, 0.4, 0.5, 0.6, 0.7, 0.8$ (**A**, **B**). Results showing effect of various Poisson's ratio, $\nu = 0, 1/4, 1/2$ (**C**, **D**).

corresponding to a decrease in radial width of the disk, for fixed outer radius (see examples of this change in geometry in Fig. 3)—also increases the disk's out-of-plane stiffness. Similarly the buckling acceleration, $\bar{\Omega}_{\text{buckle}}$, increases with angular velocity, $\bar{\omega}$. This is due to centripetal acceleration of the disk, which generates tensile (membrane) in-plane stresses—see Appendix A—that also stiffen the disk.

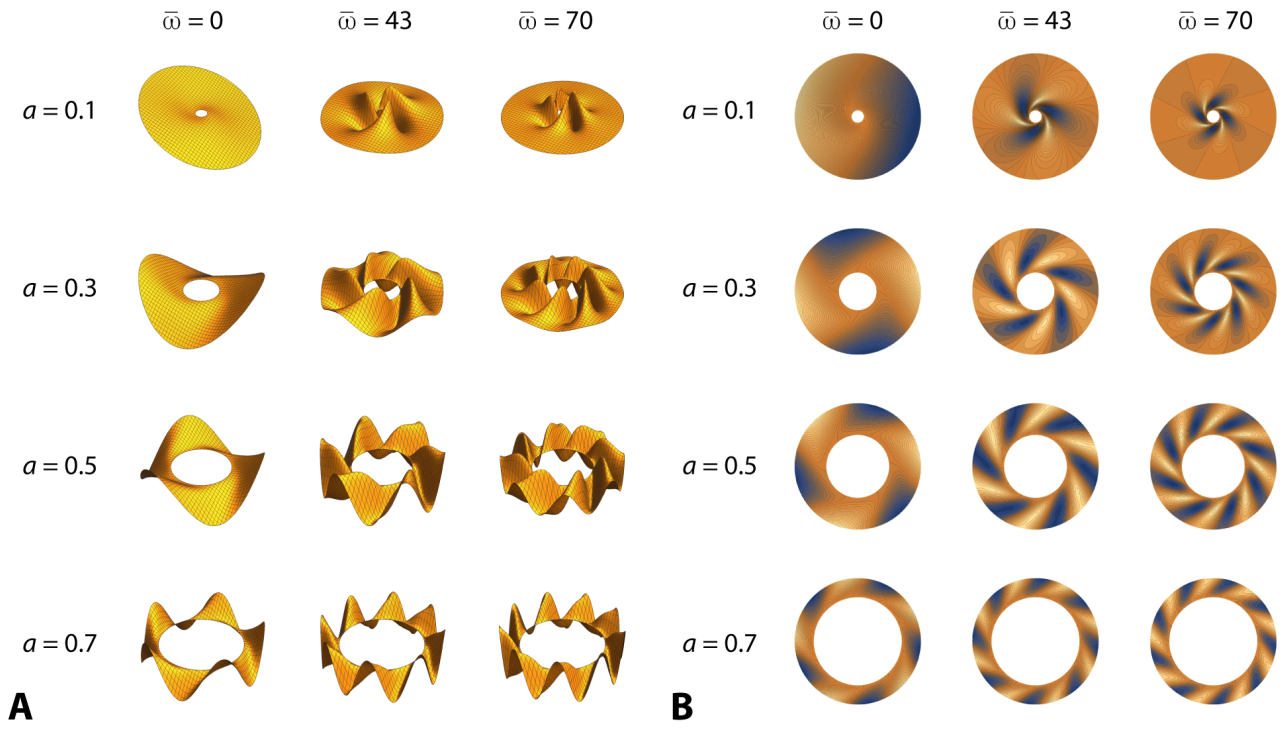

FIG. 3. Buckled mode shapes as a function of disk aspect ratio, a, and instantaneous angular velocity, $\bar{\omega}$. **A**. Three-dimensional deformation plots. **B** Corresponding contour plots. Results given for a Poisson's ratio, $\nu = 1/4$.

B. Buckled mode number

Results for the associated buckled mode numbers, n_{buckle}, are given in Figures 2(B, D) and increase with angular velocity, $\bar{\omega}$. This increase is again due to tensile in-plane stresses which serve to localize the buckled mode to the inner edge of the disk. This effect is evident in Fig. 3 and is discussed in detail next. The shear deformation of the modes is also clear with the disk accelerating (and rotating) in a counterclockwise direction. We remind the reader that the required buckled mode (observed in practice) is given by the mode with the lowest buckling acceleration.

As noted above, increasing the instantaneous angular velocity confines the buckled mode towards the disk's center. The radial extent of this deformation zone, L_{ext}, thus decreases, which in turn sets the azimuthal wavelength of the dominant buckled mode, i.e., the wavelength in the ϕ-direction; this effect is evident in Fig. 3. This reduction in azimuthal wave-

length increases the buckled mode number, n_{buckle}, which is captured by the scaling relation,

$$n_{\text{buckle}} \approx \lfloor \frac{A}{\min(1-a, L_{\text{ext}})} \rfloor, \tag{16}$$

where $\lfloor ... \rfloor$ specifies the integer part, and the constant A is expected to be order one in magnitude for dimensional reasons [29]; comparing Eq. (16) to the numerical data in Fig. 2 for $\bar{\omega} = 0$, yields good agreement with $A \approx 5/3$, for all Poisson's ratios. Note that $L_{\text{ext}} = 1-a$ for $\bar{\omega} = 0$, because the deformation zone spans the entire disk in that case; see Fig. 3.

We now examine the mechanism leading to confinement of the buckled modes towards the disk center, as the angular velocity is increased; see Fig. 3. This behavior is also observed in independent calculations for the static shear loading of an annular disk, discussed in Section I—an applied radial tension in that (different) static problem confines the buckled mode towards the inner edge of the disk, e.g., see Figs. 2, 3 and 4 of Ref. [25]. Importantly, the in-plane shear stress, $T_{r\phi}$, in the spin-up problem is generated by the angular acceleration of the disk, while the normal in-plane stresses, T_{rr} and $T_{\phi\phi}$, are due to the instantaneous angular velocity—these normal and shear components are decoupled; formulas for which are given in Appendix A. The normal stress components are always tensile and finite, see Eqs. (A2) and (A3), and act to stabilize the disk. In contrast, the shear stress increases in magnitude monotonically towards the disk's inner edge; in the limit, $a \to 0$, the shear stress is singular at the inner edge; see Eq. (A4). Thus, the disk is most susceptible to deforming near its inner edge. Increasing the instantaneous angular velocity will therefore drive the buckling deformation mode towards the inner edge of the disk—leading to the buckling mode confinement observed in Fig. 3.

Increasing the angular velocity is found to increase the number of modes that possess similar buckling accelerations. We illustrate this phenomenon by considering some numerical examples, for a disk of aspect ratio $a = 0.1$ with a Poisson's ratio $\nu = 1/4$. Accelerating the disk from rest, yields a buckled mode number of $n_{\text{buckle}} = 1$ with a buckling acceleration of $\bar{\Omega}_{\text{buckle}} = 26.0$; see upper left mode in Figs. 3(A, B). The mode with the closest buckling acceleration $\bar{\Omega} = 238$ possesses $n = 2$ (not shown). In contrast, spinning the same disk at an angular velocity of $\bar{\omega} = 70$ gives a buckled mode number of $n_{\text{buckle}} = 4$ with $\bar{\Omega}_{\text{buckle}} = 569$; upper right mode in Figs. 3(A, B). The nearest neighbor modes (with $n = 3$ and 5) have buckling accelerations of $\bar{\Omega} = 581$ and 592, respectively (again not shown); other modes have higher buckling accelerations. Consequently, the critical mode number (observed in

practice), n_{buckle}, at high angular velocity can be susceptible to non-idealities in the disk, e.g., disk imperfections and material anisotropy. This of course does not significantly affect the critical buckling acceleration, $\bar{\Omega}_{\text{buckle}}$, which is the primary variable of interest in design and application.

This similarity with respect to mode number can be understood from energy considerations, because the buckling acceleration arises from a balance of the destabilizing in-plane stresses and stabilizing bending stresses. The buckling acceleration, $\bar{\Omega}$, for any mode number, n, can be formally expressed as a ratio of the strain energies arising from these two processes (due to in-plane and bending stresses), e.g., by constructing the Rayleigh quotient of Eq. (11). For small n, which coincides with small angular velocity, the ratio of these strain energies will change significantly if the mode number n is changed by one, i.e., $n \to n+1$. This is simply because the relative change in n is large in such cases. The buckled modes themselves are also qualitatively different in this limit, which is well illustrated for the $n_{\text{buckle}} = 1, 2, 3$ modes at $\bar{\omega} = 0$ in Fig. 3 (first three rows). This highlights the difference in the ratio of the above-mentioned strain energies which depend explicitly on these mode shapes. However in the limit, $n_{\text{buckle}} \gg 1$, corresponding to high angular velocity and tight confinement of the buckled modes towards the disk center, the relative change in the ratio of these strain energies under $n \to n + 1$, is of course much smaller. The buckled modes themselves, and hence the ratio of the strain energies, are also similar; see Fig. 3. As such, the number of modes that exhibit nearly identical buckling accelerations must increase with increasing angular velocity.

For aspect ratios, a, near unity we observe that the buckled mode deformation does not decay to zero at the disk's outer edge (for the angular velocities considered in Fig. 3), i.e., $L_{\text{ext}} = 1 - a$. This produces a buckled mode whose azimuthal spatial wavelength is similar to the radial extent of the disk's annular region, which also leads to an enhanced buckled mode number, n_{buckle}, relative to disks of small aspect ratio; see Eq. (16). The buckling accelerations of modes in the limit, $a \to 1$, are close for identical reasons to those given above. That is, the buckling mode number, n_{buckle}, is high and the mode shapes are similar as n is varied around $n = n_{\text{buckle}}$; see example in Fig. 4, which shows the variation in the buckling acceleration versus mode number. We remind the reader that the mode with the smallest buckling acceleration, $\bar{\Omega}_{\text{buckle}}$, and its associated mode number, n_{buckle}, is the one observed in practice.

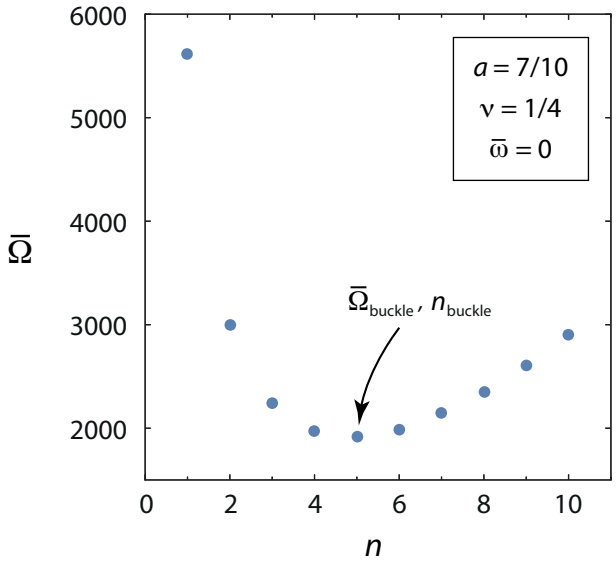

FIG. 4. Buckling accelerations, $\bar{\Omega}$, as a function of mode number, n, for a disk with $a = 0.7$, $\bar{\omega} = 0$ and $\nu = 1/4$. The required buckling acceleration and mode number for the disk, observed in practice, are specified by the lowest acceleration, $\bar{\Omega}_{\text{buckle}}$.

C. Plastic failure or elastic buckling?

We now compare the above results for shear-induced elastic buckling to existing literature for the plastic failure of a rotating and accelerating disk [18]. Both theories give a critical acceleration at which failure occurs, for a specified angular velocity, and can be used to determine the stability of thin disks. Importantly, the theory that gives the lower critical acceleration specifies the dominant failure mechanism. For a steadily rotating disk, i.e., zero angular acceleration, obviously only plastic failure remains; this is explored below.

Reid [18] theoretically studied the plastic failure of a thin disk undergoing spin-up, using the Tresca yield criterion, and reported the following yield curves (in the notation and scalings of the present study—this corresponds to Case I of Ref. [18]),

$$\begin{aligned} \sqrt{(1-\nu)^2 T_1^2 \bar{\omega}^4 + T_2^2 \bar{\Omega}^2} &= Q, \qquad \text{if } \bar{\omega}^2 \leq S\,\bar{\Omega}, \\ (1+\nu) T_1 \bar{\omega}^2 + \sqrt{(1-\nu)^2 T_1^2 \bar{\omega}^4 + T_2^2 \bar{\Omega}^2} &= 2Q, \qquad \text{if } \bar{\omega}^2 > S\,\bar{\Omega}, \end{aligned} \tag{17}$$

where Y is the tensile yield stress of the disk, and

$$T_1 = \frac{(1-a^2)\,(3+\nu+a^2[1-\nu])}{4a^2\,(1+\nu+a^2[1-\nu])}, \quad T_2 = \frac{1-a^4}{2a^4},$$

$$Q = \frac{12\,(1-\nu^2)}{a^2}\left(\frac{R}{h}\right)^2\frac{Y}{E}, \quad S = \frac{T_2}{2\sqrt{\nu}\,T_1}. \tag{18}$$

Equation (17) is easily solved to give the following explicit formula for the yield curve,

$$\bar{\Omega} = \frac{1}{T_2}\min\left(\sqrt{Q^2-(1-\nu)^2T_1^2\bar{\omega}^4},\, 2\sqrt{(Q-T_1\bar{\omega}^2)\,(Q-\nu T_1\bar{\omega}^2)}\right), \quad \text{if } \bar{\omega} \le \sqrt{\frac{Q}{T_1}}, \tag{19}$$

which specifies the maximum acceleration, $\bar{\Omega} = \bar{\Omega}_{\max}$, for a given angular velocity, $\bar{\omega}$, below which the disk deforms purely elastically; $\bar{\Omega} \ge 0$ is assumed throughout. Note that yielding occurs for all $\bar{\omega} \ge \bar{\omega}_{\max} \equiv \sqrt{Q/T_1}$, regardless of the angular acceleration, $\bar{\Omega}$, i.e., there exists a maximum angular velocity for any thin disk above which plastic failure always occurs. It is evident from Eq. (19) and the definition of Q in Eq. (18) that a thin disk, i.e., $h/R \ll 1$, is needed for elastic deformation. This is entirely consistent with a principal assumption underlying the Föppl–von Kármán equations in Eqs. (1) and (2); see discussion in Section II A.

We proceed by way of example and consider the practical case of a thin disk composed of Kapton—whose stability under steady rotation and in the presence of gravity was recently examined [7]. The Kapton disk studied in Ref. [7] has a radius-to-thickness ratio of $R/h =$ 4,000 and a tensile yield stress of $Y \approx E/20$. Figure 5(A) gives the (plastic) yield curve, Eq. (19), of this disk for the same range of disk aspect ratios, a, as in Fig. 2. The yield curve for $a = 0.02$ is the only one visible on the axes scales shown; yield curves for all other aspect ratios lie above this curve. A Poisson ratio of $\nu = 1/4$ is also used for convenience while noting that this material parameter exerts a relatively weak effect.

The curves in Fig. 5(A) for plastic failure (only $a = 0.02$ appears, see above) are to be compared to those in Fig. 2(A) for shear-induced elastic buckling, at identical values of aspect ratio, a. If the curve in Fig. 2(A) lies below the corresponding curve for $a = 0.02$ in Fig. 5(A), stability of the disk is dictated by shear-induced elastic buckling—otherwise, the disk will fail plastically as it accelerates. This comparison establishes that for the angular velocity and aspect ratio ranges used, $0 \le \bar{\omega} \le 100$ and $0.02 \le a \le 0.8$, respectively, shear-induced elastic buckling completely dictates stability, with plastic failure playing no role.

Results for a smaller radius-to-thickness ratio of $R/h = 1{,}000$, typical for a floppy-disk, are given in Fig. 5(B), which shows that all yield curves are lowered, i.e., they occur at

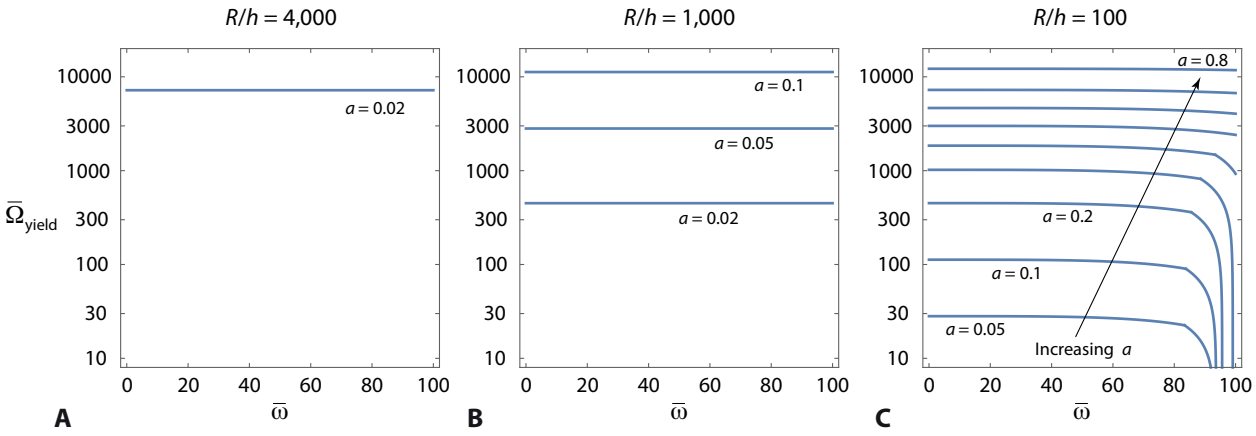

FIG. 5. Yield curves for plastic failure of a thin disk that is undergoing rotation at angular velocity, $\bar{\omega}$, and angular acceleration, $\bar{\Omega}$. Subscript 'yield' denotes the critical value for plastic failure. These curves are to be compared to results for shear-induced elastic buckling in Fig. 2(A); see text. Results given for disk aspect ratios of $a = 0.02, 0.05, 0.1, 0.2, 0.3, 0.4, 0.5, 0.6, 0.7, 0.8$, and a Poisson's ratio $\nu = 1/4$, as per Fig. 2(A); identical axes scales to Fig. 2(A) are also used to facilitate comparison. (**A**) Radius-to-thickness ratio, $R/h = 4{,}000$ [7], (**B**) $R/h = 1{,}000$, and (**C**) $R/h = 100$.

smaller angular accelerations (and smaller angular velocities, as will become evident below). Comparison of the curves in Figs. 2(A) and 5(B) still shows that all yield curves lie above the corresponding curves (at identical a) for shear-induced elastic buckling. Thus again, shear-induced buckling dictates stability for the angular velocity and aspect ratio range shown.

Figure 5(C) gives results for the even smaller radius-to-thickness ratio of $R/h = 100$, where the yield curves are lowered further; this results in very different behavior. First, we note that the yield curve for $a = 0.02$ is not visible in Fig. 5(C)—it lies below the bottom horizontal axis and therefore does not intersect the corresponding curve for shear-induced buckling in Fig. 2(A). This establishes that plastic yielding dictates the stability of this disk. In contrast, the yield curve for $a = 0.05$ in Fig. 5(C) intersects the shear-induced buckling curve in Fig. 2(A) at $\bar{\omega} \approx 4.4$. Thus, shear-induced elastic buckling governs stability for $\bar{\omega} \lesssim 4.4$ while plastic yielding controls stability above this angular velocity range. Indeed, a similar picture emerges for all larger aspect ratios studied with shear-induced elastic buckling dictating stability in the lower angular velocity range while higher angular velocities are controlled by plastic failure. Unlike the data in Figs. 5(A, B), the data in Fig. 5(C) now

clearly shows the existence of the maximum angular velocity, $\bar{\omega}_{\max}$, where the yield curves are vertical. Operation using angular velocities above this maximum value will result in plastic failure, regardless of the angular acceleration.

We remind the reader that the present analysis for shear-induced elastic buckling (and that for plastic failure [18]) implicitly assumes a large radius-to-thickness ratio, i.e., $R/h \gg 1$; see Section II A. Strictly, the radial extent of the elastic disk must greatly exceeds its thickness, i.e., $(1-a)R/h \gg 1$, which provides a stronger practical constraint on R/h especially for large aspect ratios, i.e., $a \approx 1$.

Collectively, the analysis and results reported in this section show that shear-induced elastic buckling (rather than plastic failure) can dominate the stability of many disks found in practice. This key finding has obviously implications to practical disk design and operation.

D. Comparison to a statically loaded disk

We conclude with a cautionary note. The buckled modes in Fig. 3 for an accelerating annular disk bear a resemblance to those generated by a static loaded annular disk; for example, see Refs. [19–25]. This is not surprising given both buckling phenomenon are driven by shearing mechanisms: in the present case, shear stress is due to plate inertia while for static loading the shear stress is generated by restraint of both inner and outer edges of the disk. However, the present spin-up problem induces a shear stress and radial tension in the disk that both vanish at the outer edge, due to the zero traction boundary condition at that position; namely, $\hat{\boldsymbol{r}} \cdot \mathbf{T}\,|_{r=1} = \mathbf{0}$, which gives $T_{rr} = T_{r\phi} = 0$ at $r = 1$, a property that is evident in Eqs. (A2) and (A4). This differs from existing solutions [19–25] that impose a static nonzero shear (and tension in some cases) at the outer edge of the disk, e.g., via a solid boundary, giving $T_{rr}, T_{r\phi} \neq 0$ at $r = 1$. Thus, while these spin-up and static shear problems display some qualitative similarities, they are essentially different and one cannot be derived from the other.

IV. CONCLUSION

We have studied the shear-induced buckling of a thin annular disk undergoing spin-up. Numerical results were provided as a function of the disk's aspect ratio (inner-to-outer ra-

dius), Poisson's ratio and instantaneous angular velocity. The calculations show that the buckled mode number increases with angular velocity of the disk, while the buckled deformation mode becomes progressively confined to the disk's inner edge. The number of modes with nearly identical buckling accelerations also increases with the disk's instantaneous angular velocity—this has implications to the buckled mode exhibited in practice, due to the inevitable presence of non-idealities, i.e., imperfections in the disk. This property does not significantly affect the associated buckling acceleration.

The theory and the numerical results presented here for shear-induced elastic buckling are complementary to those of the widely studied plastic failure problem. Combination of these theories is expected to find utility in engineering design and application because both mechanisms can dominate stability depending on the disk dimensions and material properties. Interestingly, the stability of practical thin disks such as floppy disks are found to be controlled by shear-induced elastic buckling rather than plastic failure.

ACKNOWLEDGEMENTS

The authors thank Debadi Chakraborty for interesting discussions and acknowledge support from the Australian Research Council Centre of Excellence in Exciton Science (CE170100026), the Australian Research Council Grants Scheme and the Northrop Grumman Corporation.

Appendix A: In-plane stress distribution

The dimensionless solution to Eqs. (2), (3) and (4), for a thin annular disk undergoing spin-up that is subject to zero radial displacement and traction at $r = a$ and $r = 1$, respectively, is [1, 16, 17]

$$\mathbf{T} = T_{rr}\hat{\boldsymbol{r}}\hat{\boldsymbol{r}} + T_{\phi\phi}\hat{\boldsymbol{\phi}}\hat{\boldsymbol{\phi}} + T_{r\phi}(\hat{\boldsymbol{r}}\hat{\boldsymbol{\phi}} + \hat{\boldsymbol{\phi}}\hat{\boldsymbol{r}}), \tag{A1}$$

where

$$T_{rr} = \frac{\left([3+\nu]\left[(1+\nu)r^2 + a^2(1-\nu)\left(1+r^2\right)\right] - a^4\left[1-\nu^2\right]\right)\left(1-r^2\right)}{8\left(1+\nu+a^2\left[1-\nu\right]\right)r^2}, \tag{A2}$$

$$T_{\phi\phi} = \frac{a^4\left(1-\nu^2\right)\left(1+r^2\right) - a^2(1-\nu)\left(3+\nu+\left[1+3\nu\right]r^4\right) + (1+\nu)\left(3+\nu-\left[1+3\nu\right]r^2\right)r^2}{8\left(1+\nu+a^2\left[1-\nu\right]\right)r^2}, \tag{A3}$$

$$T_{r\phi} = \frac{r^4 - 1}{4r^2}, \tag{A4}$$

and a is the ratio of the inner to outer radii of the disk.

---

[1] S. Timoshenko and J. N. Goodier, *Theory of Elasticity* (McGraw-Hill, New York, 1951).

[2] H. Ouyang, W. Nack, Y. Yuan, and F. Chen, "Numerical analysis of automotive disc brake squeal: a review," International Journal of Vehicle Noise and Vibration **1**, 207–231 (2005).

[3] J. E. Mottershead, "Vibration and friction-induced instability in disks," The Shock and Vibration Digest **30**, 14–31 (1998).

[4] W. D. Iwan and T. L. Moeller, "The stability of a spinning elastic disk with a transverse load system," ASME Journal of Applied Mechanics **43**, 485–490 (1976).

[5] H. P. Lee and T. Y. Ng, "Vibration and critical speeds of a spinning annular disk of varying thickness," Journal of Sound and Vibration **187**, 39–50 (1995).

[6] J.-S. Chen and Y.-Y. Fang, "Warping of stationary and rotating heavy disks," International Journal of Solids and Structures **48**, 3032–3040 (2011).

[7] M. Delapierre, D. Chakraborty, J. E. Sader, and S. Pellegrino, "Wrinkling of transversely loaded spinning membranes," International Journal of Solids and Structures **139-140**, 163–173 (2018).

[8] D. Durban and V. Birman, "Elasto-plastic analysis of an anisotropic rotating disc," Acta Mechanica **49**, 1–10 (1983).

[9] U. Gamer, "Tresca's yield condition and the rotating disk," ASME Journal of Applied Mechanics **676**, 676–678 (1983).

[10] L. H. You and J. J. Zhang, "Elastic-plastic stresses in a rotating solid disk," International Journal of Mechanics Sciences **41**, 269–282 (1999).

[11] G. Ma, H. Hao, and Y. Miyamoto, "Limit angular velocity of rotating disc with unified yield criterion," International Journal of Mechanics Sciences **43**, 1137–1153 (2001).

[12] E. Ore and D. Durban, "Elastoplastic buckling of annular plates in shear," ASME Journal of Applied Mechanics **56**, 644–651 (1989).

[13] H. Ouyang, J. E. Mottershead, M. P. Cartmell, and M. I. Friswell, "Friction-induced parametric resonances in discs: effect of a negative friction-velocity relationship," Journal of Sound

and Vibration **209**, 251–264 (1998).

[14] J.-S. Chen and D. B. Bogy, "Natural frequencies and stability of a flexible spinning disk-stationary load system with rigid-body tilting," ASME Journal of Applied Mechanics **60**, 470–477 (1993).

[15] `https://youtu.be/zs7x1Hu29Wc?t=6m46s`.

[16] M. Stern, "Rotationally symmetric plane stress distributions," Zeitschrift für Angewandte Mathematik und Mechanik **45**, 446–447 (1965).

[17] S. Tang, "Note on acceleration stress in a rotating disk," International Journal of Mechanics Sciences **12**, 205–207 (1970).

[18] S. R. Reid, "On the influence of acceleration stresses on the yielding of disks of uniform thickness," International Journal of Mechanical Sciences **14**, 755–763 (1972).

[19] W. R. Dean, "The elastic stability of an annular plate," Proceedings of the Royal Society of London. Series A **106**, 268–284 (1924).

[20] D. Durban and Y. Stavsky, "Elastic buckling of polar-orthotropic annular plates in shear," International Journal of Solids and Structures **18**, 51–58 (1982).

[21] M. Hamada and T. Harima, "In-plane torsional buckling of an annular plate," Bulletin of JSME **29**, 1089–1095 (1986).

[22] E. Reissner, "On tension field theory," Proceedings of the Fifth International Congress on Applied Mechanics , 88–92 (1938).

[23] M. Stein and J. M. Hedgepeth, *Analysis of partly wrinkled membranes*, Tech. Rep. TN D-813 (NASA, 1961).

[24] X. Li and D. J. Steigmann, "Finite plane twist of an annular membrane," Quarterly Journal of Mechanics and Applied Mathematics **46**, 601–623 (1993).

[25] C. D. Coman and A. P. Bassom, "Wrinkling of pre-stressed annular thin films under azimuthal shearing," Mathematics and Mechanics of Solids **13**, 513–531 (2008).

[26] L. D. Landau and E. M. Lifshitz, *Theory of Elasticity* (Pergamon Press, Oxford, 1970).

[27] P. G. Ciarlet, "A justification of the von Kármán equations," Archive for Rational Mechanics and Analysis **73**, 349–389 (1980).

[28] `http://library.wolfram.com/infocenter/MathSource/8762/`.

[29] P. W. Bridgman, *Dimensional Analysis* (Yale University Press, 1931) p. 615.